2018 IEEE Intelligent Vehicles Symposium (IV)
Changshu, Suzhou, China, June 26-30, 2018

A Reliable Road Segmentation and Edge Extraction for Sparse 3D Lidar Data

Jianfeng Gu, Yuehui Wang, Long Chen, Zhihao Zhao, Zhe Xuanyuan, Kai Huang*
Key Laboratory of Machine Intelligence and Advanced Computing, Ministry of Education
School of Data and Computer Science, Sun Yat-sen University
gujf5@mail2.sysu.edu.cn, wangyh83@mail2.sysu.edu.cn, chenl46@mail.sysu.edu.cn
zhaozhh25@mail2.sysu.edu.cn, zhexuanyuan@uic.edu.hk, huangk36@mail.sysu.edu.cn

***Abstract*— Precise segmentation of road areas using cheap Lidar is a tough and critical task due to data sparsity problem. With sparse point clouds, reliable perception of environment is difficult due to the lack of available information and loss of object features. This paper presents a new approach to use sparse 3D Lidar data for road segmentation by fusing multiple frames of point cloud. With registration of multiple frames into a same coordinate system, reliable data can be provided for later ground segmentation and edge extraction. The accuracies of extensive experiments on three kinds of roads demonstrate that the proposed approach obtains high precision and reliability.**

I. INTRODUCTION

Environment perception is one of the key tasks for intelligent vehicles as it provides crucial information not only for scene understanding, but also for later-on decision-making and planning. The basic component of environment perception is the detection of traversable road areas, obstacles, curbs, etc. Reliable classification and segmentation of these objects, especially the ground segmentation, enables intelligent vehicles to drive safely and efficiently.

In recent years, 3D LiDAR, which continuously launches and receives multi-beams laser at 360 degrees to obtain the precise 3D location information, becomes pervasive for environment perception. On the one hand, traditional 2D Lidar/Radar can only detect obstacles in a single scanning plane, which cannot accurately segment the ascending road. On the other hand, LiDAR-based approaches outperform those camera-based ones as cameras are sensitive to light change, lack of distance information, and inaccurate in distance measurement. Therefore, 3D LiDAR becomes an indispensable part for perception system of unmanned vehicles.

Applying 32/64 channels LiDAR in real-life usage is problematic. For those 32/64 channels LiDAR, although they can generate dense point cloud in each frame, the price of these LiDAR is however too high. For instance, 32 and 64 channel Velodyne LiDAR are about $40,000 and $80,000, respectively. Such high price is unacceptable for any civil unmanned vehicles. For LiDAR with fewer channels, the returned points of each perceived object are much sparser. With sparse point clouds, reliable perception of environment is difficult due to the lack of available information and loss of object features. In addition, if the roads are unstructured with objects of low elevation differences on the roadside, e.g., grasses or other plants, the problem would become tougher and more challenged.

Being aware that the LiDAR can generate point clouds at frequencies around 15-20 HZ, it is possible to make use of multiple consecutive frames of the point clouds for each road segmentation and edge extraction, particular for low-speed scenarios. This paper presents a new approach to use sparse 3 D LiDAR data for road segmentation for low-speed mobile robots. The basic idea of our approach is to fuse multiple frames of the point clouds to make perceived data denser. With the registration of multiple frames into a same coordinate system, reliable data can be provided for later obstacle detecting and ground segmentation. Evaluating on real-life scenarios, our approach demonstrates an excellent fitting results even with lots of noisy data. Detailed contributions of our approach can be summarized as follows.

- We develop a new approach for precise road segmentation with cheap LiDAR. Our approach consists of multiple steps, i.e., applying iterative closest point (ICP) to match the target point cloud from source point clouds, VoxelGrid filter for removing the overlapping points from the registered point cloud, LineFit algorithm to remove obstacle points with loose threshold according to their obvious vertical difference, and RANSAC (Random Sample Consensus) to extract the cloud points of road area.
- We also present a method to estimate the trend of road and extract boundary. Border points are first extracted and analyzed in curve sections and then polynomial fitting method is used to generate the boundary of roads.
- We conduct experiments with the data set acquired from a transform substation of China Southern Power Grid and evaluate the precision of the result through comparison with manually digitized ground truth.

The organization of paper is as follows. Before giving the details of our approach in Section III, we first give an outline of related work in Section II. In Section IV, we demonstrate our experiment as well as results, then conclusion of the paper is shown in Section V.

II. RELATED WORKS

In general, the methods for ground segmentation with pure 3D Lidar data, instead of Lidar-vision fuse method [1],

mainly include grid-map based method, line-based method, plane-fitting method and Lidar-imagery method.

Grip-map based method had been widely used in early DARPA Grand Challenge [2] since 2007. Within a grid, the maximum and minimum height of points were computed to generate a max-min elevation map. Based on height difference and pre-defined threshold, obstacles and ground were classified. However, the method can be easily disturbed by noise points and result in over-segmentation.

Tongtong [3] introduced an approach built on polar grid, in which points were mapped into divided sectors and ground was extracted for every sector by 1D Gaussian process regression and Incremental Sample Consensus (INSAC). Furthermore, Himmelsbch [4] presented an approach that fast projected the unordered points to polar grid to construct the neighborhood relation for further sophisticated feature extraction. This method failed to precisely segment the road area due to less sensitivity to low height obstacles, like grasses and rocks. But it performed especially well in obstacle segmentation even with loose thresholds.

Line-based method mainly focuses on the features of one spin, relations between neighboring spins or scan lines [5]. The representation of features includes gradient, normal vectors, radial and tangential angle features, local convexity criterion et al. M. Li [6] proposed a method of Four Directions Scan Line Gradient Criterion (4DSG) that calculated the difference, variance, and the gradient variation in four directions within a basic grid unit to extract single scan line features. Based on these features, roads, curbs and obstacles were classified. Besides, J. Cheng [7] presented a Ring Gradient-based Local Optimal Segmentation (RGLOS) algorithm to extract gradient feature between scan lines. However, these approaches to extract features are mostly based on the dense point cloud data and their experiments are supported by 64 lasers Lidar.

In most practical situations, the ground is known to be relatively flat, like asphalt pavement and slabstone road. Plane-fitting method has proven to possess a great performance in ground surface abstraction, especially the algorithm of Random Sample Consensus (RANSAC), provided that the data captured from Lidar is dense enough. K. Qiu [8] extracted a rough plane based on RANSAC algorithm with dense data set, and then refined the plane according to road width and continuity. J. Lam et al. [9] applied RANSAC and least squares fitting method to extract the ground surface in local point clouds, which worked effectively.

Lidar-imagery based method focuses on projecting Lidar points into a certain image plane which retains the original 3D information and utilizes image processing methods to segment the ground. L. Chen [10] proposed a Lidar-imagery based disparity method to find the road plane by converting the distance values to disparity values. Recently, deep learning methods [11], [12] were applied to segment the ground by training FCN and CNN. But these methods also required the dense Lidar data.

Combination of various effective methods is a trend of ground segmentation when confronting different road conditions. R. Huang [5] and J. Liu [13] detected the driving region and curb by a multi-feature extraction framework including feature of maximum height difference in a grid, radial gradient, etc. In our method, Linefit, a grid-map and line based method, and RANSAC, a plane based method, have been adopted to ensure the reliability of ground segmentation.

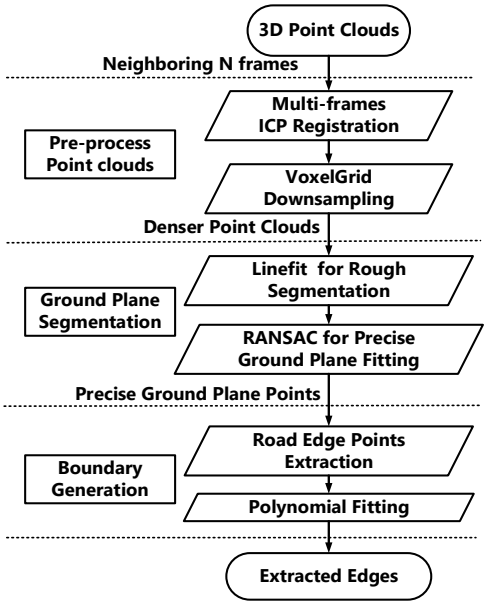

Fig. 1. Framework of road segmentation and edge extraction.

III. FRAMEWORK

Our proposed framework is composed of pre-process of point cloud, ground plane segmentation and road boundaries generation, shown in Fig. 1. Firstly, we capture neighboring N-frame point clouds and utilize fast ICP to make the point cloud denser. Meanwhile, VoxelGrid filter can remove the redundant overlapping points after registration. Then the model Linefit and robust plane fitting algorithm RANSAC are applied to roughly and precisely segment the ground plane, respectively. Finally, based on the ground point cloud, we extract the road edge points and generate road boundary by polynomial fitting.

A. ICP Registration for Improving Density and VoxelGird Filter

Iterative Closest Point (ICP) is an algorithm employed to minimize the difference of two point clouds, and it is widely applied for point cloud registration. Here we apply multi-frame ICP to make perceived point clouds denser. Given two point clouds, $X = \{x_i\}_{i=1}^{N_x}$ and $Y = \{y_j\}_{j=1}^{N_y}$, where N_x and N_y denote the number of points in cloud X and Y, respectively, X is kept fixed as target point cloud while the point cloud Y, the source, is transformed to best match it. For each point y_i in Y, ICP finds a corresponding closest point x_j in X. Least square (LS) is employed to represent the distance of two point clouds, which is shown in following representation.

$$\begin{cases} \min\limits_{R,T,j\in\{1,2,\ldots,N_x\}} \left(\sum\limits_{i=1}^{N_y} \|(Ry_i + T) - x_j\|_2^2 \right) \\ s.t. \qquad R^T R = I_n, det(R) = 1 \end{cases} \tag{1}$$

where R is rotation matrix and T is translation vector, described as RT. The algorithm contains two basic steps.

- ***Step 1.*** Find the closest point pairs. According to known rigid transformation RT which is obtained in k^{th} step, we transform the Y by $R_k Y_i + T_k$ and construct the relation with X. The pair point index of y_i is:

$$c_{k+1}(i) = \underset{j \in \{1,2,\ldots,N_x\}}{\arg\min} ((\|R_k y_i + T_k) - x_j\|_2^2), i = 1, 2, \ldots, N_y \tag{2}$$

- ***Step 2.*** Revise the RT rigid transformation.

$$(R_{k+1}, T_{k+1}) = \underset{R_{k+1}^T R_{k+1} = I_n, det(R) = 1, T_{k+1}}{\arg\min} (\sum_{i=1}^{N_y} \left\| R_{k+1} y_i + T_{k+1} - x_{c_{k+1}((i))} \right\|_2^2) \tag{3}$$

K-d tree is applied to accelerate corresponding points' finding and singular value decomposition (SVD) is used to revise RT. ICP iterates in these two steps until it meets pre-defined terminal conditions like minimum difference of RT between two iterations or maximum iteration times. According to the algorithm, the initial RT will determinate the accuracy and speed of registration. Considering the practical point clouds acquired from Lidar, neighboring frames of point clouds generally have small change of rotation but more in translation. Therefore, R is initialized to identity matrix, and initialization of translation matrix T relies on the speed of vehicles and distance to the target point cloud. Based on these optimizations, the maximum iteration times are reduced to the level of single digit.

We capture multiple frames of point clouds from Lidar in real time and define the latest frame as target point cloud and others as sources to match the target. The result, working in different number of frames, are shown in Fig. 2. As shown in the figure, the original data are so sparse that the road areas are only presented by some thin curve lines. In a scene, most points are static objects, which have fixed relative position. After registration of most static objects, the change of dynamic objects will be recorded and density of static objects will be improved. For a vehicle, the ground points will be expanded in the moving direction. The expansion has produced the similar ground perception effect as higher lasers Lidar and correctly presented the trend of the road.

After multi-frame registration, the point cloud contains lots of overlapping points, which greatly increases the unnecessary computation since LineFit (a following model) applies pointwise mapping. To tackle this problem, VoxelGrid filter is introduced to down-sample the point cloud. The 3D space is divided to a set of equal voxels, which can be regarded as tiny 3D box in space. In each voxel, all the points present will be approximated with their centroid. By correctly setting the size of voxel, the overlapping points can be effectively removed.

B. LineFit for Obstacle Removing and Rough Segmentation

Obstacles detection and removing is a significant component of ground segmentation. Most obstacles share the same feature of obvious vertical difference while roads are flat or with gradual height change such as uphill and downhill, which can be easily recognized as obstacles in previous height-based segmentation methods. Himmelsbach [4] presented a fast segmentation model, which contains the approaches of polar grid mapping, total-least-squares(TLS) for lines fitting in radial direction and ground points evaluation. Our Linefit method is based on this model due to its great sensitivity to obvious obstacles.

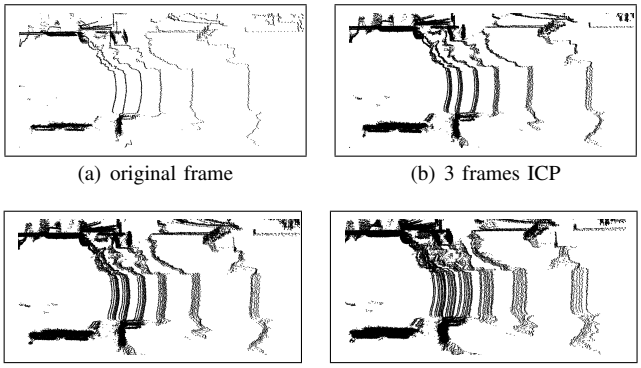

(a) original frame (b) 3 frames ICP

(c) 5 frames ICP (d) 7 frames ICP

Fig. 2. The result of ICP registration from original point cloud (a) with different number of neighboring frames.

Similar to Himmelsbash's approach, we regard the Lidar's detectable areas as a circle with a certain radius in xy-plane (ground plane). Then the circle is divided to $M(M = \frac{2\pi}{\Delta\alpha})$ equal sectors, namely segments,

$$segment(p_i) = \frac{\arctan(y_i/x_i)}{\Delta\alpha} \tag{4}$$

where p_i denotes a 3D point, $\Delta\alpha$ is the angle that every segment covers. Each segment is uniformly divided to certain number of bins in the radial direction,

$$bin(p_i) = \frac{\sqrt{x_i^2 + y_i^2} - r_{min}}{N_{bin}} (r_{min} \leq \sqrt{x_i^2 + y_i^2} \leq r_{max}) \tag{5}$$

where r_{min} and r_{max} denote the minimum and maximum radius, and N_{bin} is the number of equal bins. The spatial points are mapped to corresponding segments as well as bins to construct a new set of 2D points with transformation from (x, y, z) to $(\sqrt{x^2 + y^2}, z)$. Prototype points (the lowest z-coordinate points) are selected to represent the other points in a bin. Within a segment, linear total-least-square (TLS) model, $y = mx + b$, is applied to fit the prototype points and generate ground planes lines, shown in Fig. 3. The green lines are fitting lines, which are generated by TLS model. Finally, we evaluate the distance between the points and the lines, and label the points as ground if distance is below a threshold T_{ground} and non-ground otherwise. The method Linefit focuses on obvious obstacles removing and rough ground plane extraction so that the thresholds, including slope scope (m) of fitting lines, maximum starting height and maximum fitting error, are set to be loose to avoid over-segmentation of ramps and under-segmentation of obvious obstacle points.

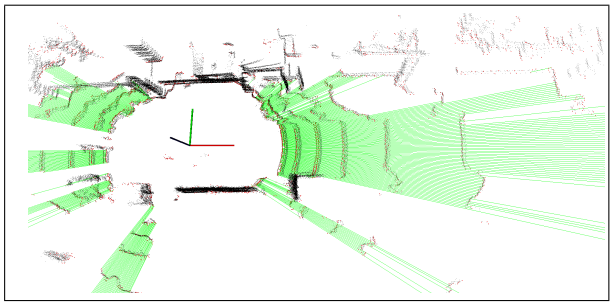

Fig. 3. Green lines denote the fitting lines of model Linefit, the red points represent the minimum-z point in a bin.

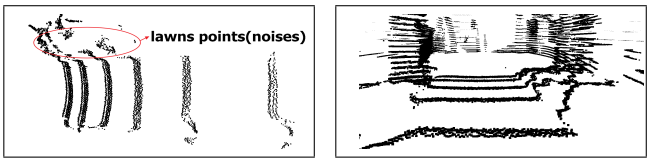

(a) Disturbance of lawn points (b) Obvious break

Fig. 4. Under-segmentation of ground with disturbance of lawn points and their difference.

C. RANSAC for Precise Ground Plane Extraction

Most of the points filtered by Linefit belong to ground plane. To tackle the disturbance of small elevation objects by the roads, such as lawns, vegetation and rocks, we apply a robust fitting algorithm, RANSAC [14], to accurately abstract the ground plane. As shown in Fig. 4(a), after using the Linefit method, some lawn points near the road fail to be removed because of the surface similarity between the lawn plane and road plane in the radial direction. However, when projected onto the ground plane, the points generated by one beam form a circle, which means that the distance of neighboring ground points are nearly the same. The distance becomes smaller when point is projected onto the positive obstacle such as grasses. Therefore, we can distinguish the lawn and the road by applying RANSAC algorithm because there must be breaks and height differences between the ground and lawn, which is shown in Fig. 4(b). We first fit a plane Π_0 based on random sampled points. For all points, if the distance $D_i(X_i, \Pi_0)$ of a point X_i to the plane Π_0 is larger than a threshold λ, the point X_i is identified as outliers, otherwise as inliers. The condition is presented as

$$D_i(X_i, \Pi_0) < \lambda \tag{6}$$

According to the ratio of inliers and outliers, the algorithm iterates in the previous steps and obtain a refined planes Π_i with larger inliers rate and lower variance. The refined plane is presented in Fig. 5.

D. Road Edge Points Extraction and Boundary Fitting

For the intelligent vehicles, the most efficient way to ensure the traversable areas quickly is to acquire roads' boundary, especially for the roads without curbs. In order to generate the boundaries, two key steps are included.

The first step is to accurately extract road edge points. In the direction of moving vehicle, lots of curve sections,

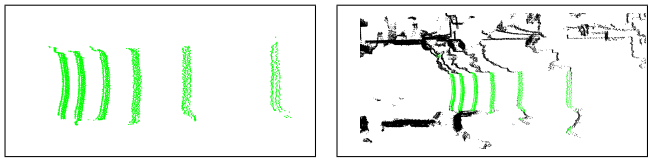

(a) Refined ground plane (b) Panorama view

Fig. 5. Precise ground segmentation with RANSAC.

which are perpendicular to xy-plane and have a fixed interval distance $T_{k+1} - T_k$, are inserted in extracted ground points. The model is displayed in Fig. 6(a). The points within two neighboring sections are mapped to the front section T_k by transforming $P_i(x_i, y_i, z_i)$, where $T_k \leq \sqrt{x_i^2 + y_i^2} \leq T_{k+1}$, to $P_i^{'}(y_i, z_i)$. The mapping result of a section is presented in Fig. 6(b).

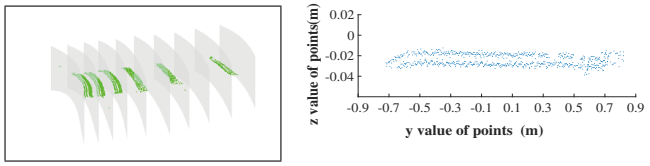

(a) Curve section model (b) Mapped points in a interval

Fig. 6. Section model and mapping.

To obtain the ranges of border points, we apply a sliding window of fixed size to scan the mapping data in most dense z band and learn the both left-most and right-most border ranges in y coordinate. Moreover, the selected left-most (or right-most) ranges must possess multiple successive non-empty windows in the right (or left) to avoid the disturbance of discrete noise points. Back to the ground point cloud, the points within the left-most and right-most border ranges are regarded as candidate border points, which are shown in Fig. 7(a). To improve reliability of extracted border points, Gaussian distribution is introduced to estimate the road widths in a section so as to avoid wrong estimations of border ranges.

Secondly, based on all extracted border points, quadratic polynomial curve fitting method is used to generate the right and left road boundaries, respectively, the result of which is presented as Fig. 7(b).

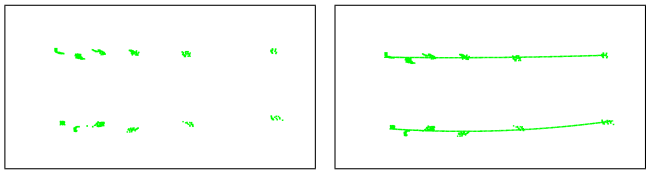

(a) Extracted border points (b) Polynomial fitting

Fig. 7. Border points' extraction and road edge extraction.

IV. EXPERIMENTS

We evaluate our approach with a low-speed surveillant robot on different road scenarios in an electricity substation, as shown in Fig. 8. The robot is equipped with Velodyne VLP-16 LiDAR and mini PC with Intel Core i7-6700 CPU and 8.0G of RAM.

Fig. 8. Autonomous surveillant robot and the unstructured asphalt road without curbs.

A. Datasets and Validation Approach

We selected three kinds of roads in different environments, including asphalt road with low-height lawns by the road (road 1), asphalt road with low-height vegetation by the road (road 2), slabstone road with low-height lawns and rocks by the roads (road 3), to evaluate our framework. The roads were all unstructured with no curbs, and there was small elevation difference at the edge of the road.

We validated our results of ground segmentation and boundary extraction through comparison with manually digitized ground truth and edges in each road sections, shown in Fig. 9. The points between the manually labeled left and right edges were considered as ground truth points. The indexes of Precision, Recall and F1 were computed to evaluate the quality of segmentation. To evaluate the precision of edge extraction, buffer zones were created around the manually digitized left and right edges in each road section. The model was widely used in evaluation of road edges extraction [8], [15]. The extracted border points and edge points within the buffers were all considered as candidate edge components, and corresponding accuracies were computed.

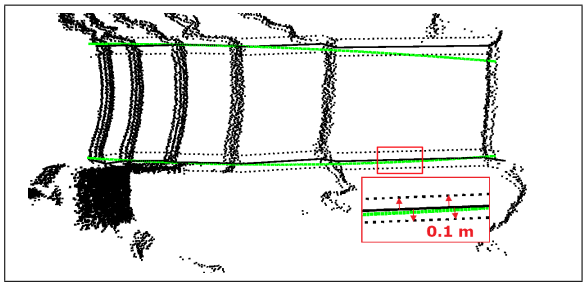

Fig. 9. The black full lines denote the manually digitized road edges. Buffer zones are presented by dotted lines, and their width(β) is 0.2m.

B. Parameters

The parameters of our experiment were shown in Table I. In the experiment, considering running time and accuracy, we used 4 neighboring frames to make the point cloud denser by the fast ICP. The latest point cloud was set to be the target point cloud and others was considered as sources. In the part of Linefit, the parameters were relatively loose for rough ground segmentation and obvious obstacle removing. The threshold λ in point-to-plane fitting relied on the smoothness of practical roads. With different width β of buffer zones, the precision of border point extraction and boundary generation would vary. Referring to previous evaluation of the edge extraction [8], [15] and the practical application, the width was set to be 0.2m.

TABLE I
THRESHOLD FOR EXPERIMENT

Part	Index	Threshold
Pre-Process	Number of ICP Frames	4
	ICP Maximum Iteration Times	15
	VoxelGrid Leaf Size	(0.01,0.01,0.01)
LineFit	Number of Segments	1000
	Number of Bins	50
	Sensor Height	0.55m
	Fitting Error	<0.10
	r_{min},r_{max}	0.5m,15m
	T_{ground}	0.05m
	Slope Range	-0.3 to 0.3
RANSAC	λ	0.03m
Evaluation	Width of Buffer Zone β	0.2

C. Evaluation

Figs. 10 to 12 demonstrated the results of applying our framework. As shown in the figures, our framework can successful segment the road areas and extract the boundaries for all three scenarios. Almost all the ground points were precisely classified, though a little misclassification existed near the boundaries of roads. As shown in Fig. 10 to 12, after registration of original frame (a), the cloud points of ground plane extended in the direction of moving vehicle and obstacle points became denser (b). The ground points (c) were precisely segmented and road edges (d) were accurately generated. In the road 1 and road 3, the end of road edges existed small deviation since the density of points gradually declined with the increasing of sensible distance, and the lawn points had great similarity to the road points at the boundaries. However, due to the advantage of denser point clouds, the disturbance had little influence on the edge generation.

We randomly selected 10 sections of each kind of roads to calculated the index of F1, Precision, Recall of segmentation, Precision of extracted border points, and Precision of boundaries extraction. The results were presented in Table II. The Precision and Recall were all near or above 90%, and F1 were over 90%. For relatively higher obstacles (vegetation) along the edges of road (road 2, Fig. 11), the framework performed excellently in both road areas segmentation and boundary extraction, which nearly reached to 95%. The average single-thread performance was about 400 milliseconds per frame.

V. CONCLUSION

In the paper, we have presented a novel approach to segment the unstructured roads with sparse point clouds acquired from lower lasers Lidar and extract the road edges. Our framework focused on the segmentation of roads, which had small elevation difference along the road edges and didn't have curbs. Meanwhile, we only used low lasers Lidar (VLP16) and sparse data to achieve the goal. With ICP registration improving the density of environment, ground segmentation and edges extraction became easier and more reliable since it provided stable foundation for the model of Linefit and ground fitting algorithm RANSAC. Furthermore,

TABLE II

THE RESULT OF ROAD SEGMENTATION AND EDGE EXTRACTION

road types	Road Segmentation(%)			Edge Extration (%)		Time(ms/frame)
	F1	Precision	Recall	Precision of Border points	Precision of Boundary Extraction	
road 1	90.17	93.10	87.42	88.12	90.35	
road 2	94.93	98.04	92.01	82.67	94.22	400
road 3	90.92	91.67	90.23	99.37	89.25	

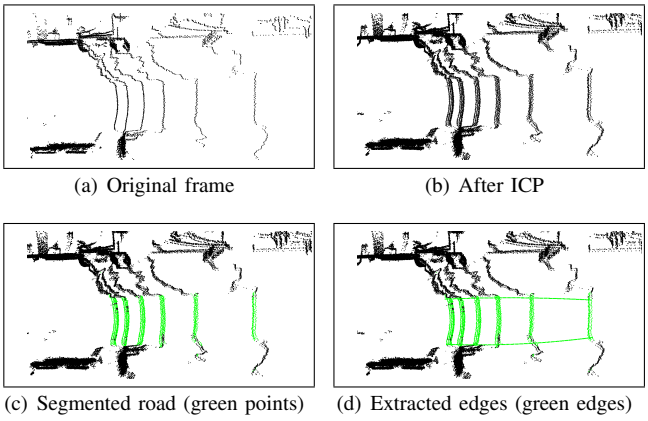

(a) Original frame (b) After ICP

(c) Segmented road (green points) (d) Extracted edges (green edges)

Fig. 10. Results of a random section in asphalt road with low-height lawns by the road.

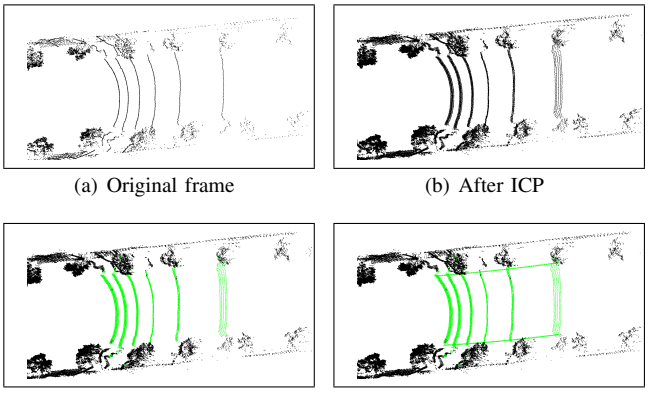

(a) Original frame (b) After ICP

(c) Segmented road (green points) (d) Extracted edges (green edges)

Fig. 11. Results of a section in asphalt road with low-height vegetation by the road.

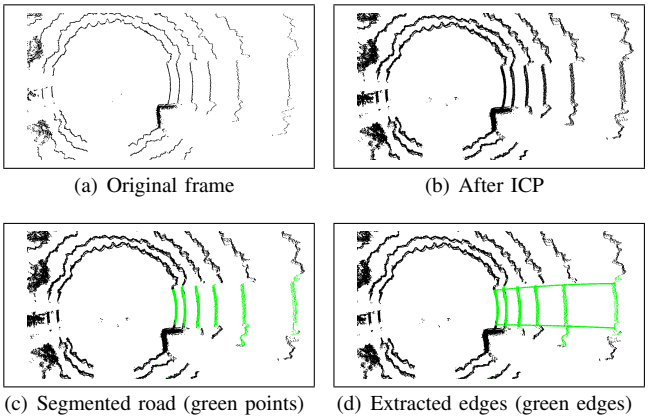

(a) Original frame (b) After ICP

(c) Segmented road (green points) (d) Extracted edges (green edges)

Fig. 12. Results of a section in slabstone road with low-height vegetation by the road.

the reliability of extracted border points was enhanced due to more selectable border points. The result of experiments in three kinds of roads has proven the excellent reliability and robustness of the approach.

ACKNOWLEDGMENT

This work was supported in part by the National Key Research and Development Program of China under grant No.2017YFB1001703; the National Science Foundation of China under Grant No. U1711265; the Fundamental Research Funds for the Central Universities under grant No.17lgjc40; the Innovative R&D Team Introduction Program of Guangdong Province.

REFERENCES

[1] Q. Li, L. Chen, and M. Li, "A sensor-fusion drivable-region and lane-detection system for autonomous vehicle navigation in challenging road scenarios," *IEEE Transactions on Vehicular Technology*, vol. 63, no. 2, pp. 540–555, 2014.

[2] C. Urmson, J. Anhalt, D. Bagnell, C. Baker, R. Bittner, M. Clark, J. Dolan, D. Duggins, T. Galatali, C. Geyer, *et al.*, "Autonomous driving in urban environments: Boss and the urban challenge," *Journal of Field Robotics*, vol. 25, no. 8, pp. 425–466, 2008.

[3] C. Tongtong, D. Bin, L. Daxue, Z. Bo, and L. Qixu, "3d lidar-based ground segmentation," in *Pattern Recognition (ACPR), 2011 First Asian Conference on*, pp. 446–450, IEEE, 2011.

[4] M. Himmelsbach, F. V. Hundelshausen, and H.-J. Wuensche, "Fast segmentation of 3d point clouds for ground vehicles," in *Intelligent Vehicles Symposium (IV), 2010 IEEE*, pp. 560–565, IEEE, 2010.

[5] R. Huang, J. Chen, J. Liu, L. Liu, B. Yu, and Y. Wu, "A practical point cloud based road curb detection method for autonomous vehicle," *Information*, vol. 8, no. 3, p. 93, 2017.

[6] M. Li and Q. Li, "Real-time road detection in 3d point clouds using four directions scan line gradient criterion," *Future*, vol. 5, 2009.

[7] J. Cheng, Z. Xiang, T. Cao, and J. Liu, "Robust vehicle detection using 3d lidar under complex urban environment," in *Robotics and Automation (ICRA), 2014 IEEE International Conference on*, pp. 691–696, IEEE.

[8] K. Qiu and K. Sun, "A fast and robust algorithm for road edges extraction from lidar data.," *International Archives of the Photogrammetry, Remote Sensing & Spatial Information Sciences*, vol. 41, 2016.

[9] J. Lam, K. Kusevic, P. Mrstik, R. Harrap, and M. Greenspan, "Urban scene extraction from mobile ground based lidar data," in *Proceedings of 3DPVT*, pp. 1–8, 2010.

[10] L. Chen, J. Yang, and H. Kong, "Lidar-histogram for fast road and obstacle detection," in *Robotics and Automation (ICRA), 2017 IEEE International Conference on*, pp. 1343–1348, IEEE, 2017.

[11] M. Velas, M. Spanel, M. Hradis, and A. Herout, "Cnn for very fast ground segmentation in velodyne lidar data," *arXiv preprint arXiv:1709.02128*, 2017.

[12] L. Caltagirone and S. Scheidegger, "Fast lidar-based road detection using fully convolutional neural networks," in *Intelligent Vehicles Symposium (IV), 2017 IEEE*, pp. 1019–1024, IEEE, 2017.

[13] J. Liu, H. Liang, Z. Wang, and X. Chen, "A framework for applying point clouds grabbed by multi-beam lidar in perceiving the driving environment," *Sensors*, vol. 15, no. 9, pp. 21931–21956, 2015.

[14] M. Fischer, "A paradigm for model fitting with applications to image analysis and automated cartography," *Comm. ACM*, vol. 24, no. 6, pp. 381–395, 1981.

[15] P. Kumar and C. P. McElhinney, "An automated algorithm for extracting road edges from terrestrial mobile lidar data," *ISPRS Journal of Photogrammetry and Remote Sensing*, vol. 85, pp. 44–55, 2013.